Energy & Environmental Science

PAPER

View Article Online
View Journal | View Issue

Cite this: *Energy Environ. Sci.*, 2015, **8**, 1501

A thermodynamic tank model for studying the effect of higher hydrocarbons on natural gas storage in metal–organic frameworks†

Hongda Zhang,[a] Pravas Deria,[b] Omar K. Farha,[bc] Joseph T. Hupp[b] and Randall Q. Snurr*[a]

Received 12th March 2015,
Accepted 7th April 2015

DOI: 10.1039/c5ee00808e

www.rsc.org/ees

Metal–organic frameworks (MOFs) are promising materials for storing natural gas in vehicular applications. Evaluation of these materials has focused on adsorption of pure methane, although commercial natural gas also contains small amounts of higher hydrocarbons such as ethane and propane, which adsorb more strongly than methane. There is, thus, a possibility that these higher hydrocarbons will accumulate in the MOF after multiple operating (adsorption/desorption) cycles, and reduce the storage capacity. To study the net effect of ethane and propane on the performance of an adsorbed natural gas (ANG) tank, we developed a mathematical model based on thermodynamics and mass balance equations that describes the state of the tank at any instant. The required inputs are the pure-component isotherms, and mixture adsorption data are calculated using the Ideal Adsorbed Solution Theory (IAST). We focused on how the "deliverable energy" provided by the ANG tank to the engine changed over 200 operating cycles for a sample of 120 MOF structures. We found that, with any MOF, the ANG tank performance monotonically declines during early operating cycles until a "cyclic steady state" is reached. We determined that the best materials when the fuel is 100% methane are not necessarily the best when the fuel includes ethane and propane. Among the materials tested, some top MOFs are MOF-143 > NU-800 > IRMOF-14 > IRMOF-20 > MIL-100 > NU-125 > IRMOF-1 > NU-111. MOF-143 is predicted to deliver 5.43 MJ L^{-1} of tank to the engine once the cyclic steady state is reached. The model also provided insights that can assist in future work to discover more promising adsorbent materials for natural gas storage.

Broader context

Natural gas is quite abundant and cheap in many parts of the world. It burns cleanly and generates less CO_2 per unit of energy than other fossil fuels. However, there are significant hurdles to the adoption of natural gas for transportation. Current natural gas vehicles mostly use compressed natural gas (CNG), where the gas is stored at 250 bar. This high pressure requires expensive, thick-walled storage tanks and imposes a significant energy cost for compression. Storing natural gas at lower pressure by filling the storage tank with a porous adsorbent material would lower the compression and vessel costs. In this work, a theoretical model was created to address the effect of the higher hydrocarbons, especially ethane and propane, on metal–organic framework (MOF) adsorbents used in an adsorbed natural gas (ANG) tank and to evaluate the performance of the materials over many adsorption/desorption cycles. The effect of these higher hydrocarbons cannot be neglected, and the result of this work could change our previous understanding of what is a good MOF for natural gas storage. The model can serve as a useful tool and provide important guidelines for future screening and design of MOF materials for natural gas storage.

[a] *Department of Chemical and Biological Engineering, Northwestern University, 2145 Sheridan Road, Evanston, Illinois 60208, USA. E-mail: snurr@northwestern.edu*
[b] *Department of Chemistry and International Institute for Nanotechnology, Northwestern University, 2145 Sheridan Road, Evanston, Illinois 60208, USA*
[c] *Department of Chemistry, Faculty of Science, King Abdulaziz University, Jeddah, Saudi Arabia*

† Electronic supplementary information (ESI) available: Experimental methane, ethane and propane single-component isotherms in HKUST-1 at 298 K (Fig. S1); correlation between the selectivity of hexane isomers calculated from full mixture simulations and from IAST at 433 K and 1 bar in 10 zeolites and MOFs (Fig. S2); the relative differences of loadings from mixture simulations and IAST calculations at 433 K and 1 bar (Table S1); comparison between the deliverable energy of the first cycle for natural gas and for pure methane in the five selected MOFs (Fig. S3); calculated PSD of HKUST-1 (Fig. S4); snapshot of adsorbed methane, ethane and propane molecules in HKUST-1 in GCMC mixture simulation at 5.8 bar and 298 K (Fig. S5); additional correlations between the deliverable energy and the MOF properties based on the screening of the 120 synthesized MOFs (Fig. S6–S9); the methane uptake and deliverable energy data of 120 screened MOFs (Table S2); Matlab routine for the ANG tank model. See DOI: 10.1039/c5ee00808e

Introduction

The continuous increase of carbon dioxide levels in the atmosphere due to burning of fossil fuels is one of today's most critical global environmental problems and is driving an intense search for alternative fuels. Natural gas (NG), which is widely abundant and mainly composed of methane, has been considered as a promising "bridge" fuel: a midterm solution to help transition to carbon-free fuels. Natural gas is already used for heating and generating electricity, but is not yet widely used for transportation, although it produces 25% less carbon dioxide when burned than conventional gasoline or diesel. The challenge for vehicular applications is that at standard temperature and pressure the volumetric energy density of natural gas is much lower than that of gasoline. Therefore, the search for efficient natural gas storage methods has been a hot topic in recent decades. Current storage techniques, such as compressed natural gas (CNG) and liquefied natural gas (LNG), suffer from safety concerns and high cost due to the extreme operating conditions: 250 bar for CNG and 111 K for LNG. An attractive solution is to use an adsorbed natural gas (ANG) system, in which porous materials are used to store natural gas at high (energy) densities under relatively mild conditions, typically ambient temperature and low pressures in the 35–65 bar range, which can be easily achieved with a two-stage compressor. The development of a promising adsorbent material is thus critical for the widespread application of ANG.

For such materials, the Advanced Research Projects Agency-Energy (ARPA-E) has recently established an adsorption target that the "deliverable energy" should reach a density of 9.0 MJ L^{-1} of tank, which is comparable to the deliverable energy of CNG at 250 bar.[1] Assuming no packing loss, this target translates into an ambitious volumetric methane deliverable capacity of 263 cc(STP) per cc of adsorbent (STP: 273.15 K, 101.325 kPa). To estimate deliverable energies, here we focus on a storage pressure of 65 bar and a delivery pressure of 5.8 bar, which is determined by the inlet pressure to the engine.[1] Some conventional porous materials such as zeolites and activated carbons have been studied in the past, although the best reported methane volumetric uptakes are quite low.[2,3]

A new class of promising crystalline nanoporous materials for natural gas storage, metal–organic frameworks (MOFs), possess the advantage of being remarkably tunable simply by selecting the appropriate combination – among millions of possibilities – of inorganic metal "nodes" and organic "linkers".[4,5] The first demonstration of methane adsorption in MOFs was reported in 1997,[6] and since then MOFs with high methane capacity have been actively pursued by many research groups.[7–20] Interestingly, due to the refinement of MOF synthesis and activation techniques, the well-known MOFs HKUST-1 and IRMOF-1 have been "rediscovered" as two of the best materials, with deliverable capacities of ~185 cc(STP) per cc of adsorbent between 65 bar and 5.8 bar.[10,15] Also, several research groups, including ours, have developed new MOFs with high methane deliverable capacities, including ZJU-25,[21] UTSA-76a,[22] NU-111,[23] NU-125,[24] NU-800[25] and MOF-519.[26] Computational work also suggests that deliverable capacities as high as 206 cc(STP) per cc of adsorbent can be reached in MOFs and similar porous materials at these operating conditions.[27–29]

In addition to methane, commercial natural gas contains small amounts of other species, such as ethane and propane. Considering only these hydrocarbons, the average molar composition of natural gas is 96% methane, 3.3% ethane and 0.7% propane.[30] Although the mole fractions of these higher hydrocarbons are low, they can have a significant effect on the performance of the adsorbent. First, due to their stronger interactions with the MOF pore walls, they adsorb more readily than methane and are more difficult to desorb. They could, thus, accumulate inside the MOF pores over multiple cycles of filling and emptying. Lucena *et al.* used grand canonical Monte Carlo (GCMC) simulations to study C1 to C4 alkane adsorption in activated carbons.[31] Rios *et al.* also carried out a series of experiments studying the effect of the higher hydrocarbons on the charge/discharge cycles in an activated carbon based ANG system.[32] They both observed the accumulation of the higher alkanes and claimed that this effect would severely decrease the efficiency of the ANG system. It should also be noted that, due to their higher molar heats of combustion (methane: −890 kJ mol^{-1}; ethane: −1560 kJ mol^{-1}; propane: −2204 kJ mol^{-1}),[33] higher hydrocarbons could increase the energy delivered to the engine compared to pure methane. Therefore, to evaluate materials for utilization in ANG tanks, it is not enough to focus solely on methane adsorption.

To study the effect of higher hydrocarbons on the performance of a large number of candidate MOF materials for ANG systems, it is important to have an accurate computational model that can predict the adsorption and desorption of realistic gaseous fuel mixtures in the tank, without conducting time-consuming and expensive natural gas cycling experiments. Hardy *et al.*[34] developed a model of an adsorption-based hydrogen storage system considering adsorption and diffusion of pure hydrogen. Farzaneh-Gord *et al.*[35,36] reported a thermodynamic analysis of the filling process for natural gas vehicle cylinders, but only focused on CNG systems, *i.e.* no adsorbent materials were considered. Thus, to date, no model has been reported to describe the performance of an ANG tank system to assess the importance of higher alkanes on the system performance.

GCMC simulation is a common approach to study gas adsorption in porous materials.[8,20,31] GCMC simulations predict the adsorption thermodynamics, *i.e.*, the amount adsorbed when the porous material is at equilibrium with a gas phase of a given temperature, pressure, and composition. This information is critical to the design and assessment of materials for natural gas storage, but it is not sufficient by itself as it does not reflect the cyclic filling and emptying of the tank and the changes in composition within both the adsorbed phase and the gas phase inside the tank during these cycles. In this work, we have developed a computationally efficient mathematical model of an ANG tank that is capable of describing the simultaneous changes in the compositions of the two phases over many adsorption/desorption operating cycles. In particular, the model is able to describe possible accumulation of more strongly adsorbed species within an ANG tank over many operating cycles. The model requires single-component adsorption isotherms, either from

experiment or molecular simulation, as inputs. We used this model to study the performance of an ANG tank for 120 MOF materials at realistic operating conditions considering the effect of ethane and propane. Our work provides new and useful information for the design of materials for ANG applications from an engineering point of view.

Model and computational details

At its core, the ANG tank model presented here is comprised of a consistent system of non-linear equations stating thermodynamic equilibrium and mass conservation principles. Solution of the model requires methane–ethane–propane mixture isotherm data for any composition of the gas phase (which varies during equilibration inside the tank). To provide these data to the model efficiently, we use the Ideal Adsorbed Solution Theory (IAST) to estimate the ternary mixture isotherms from single-component isotherms obtained from GCMC simulations (most cases) or experimental measurements (HKUST-1).

Ideal adsorbed solution theory (IAST)

Determining the adsorption behavior of mixtures for any arbitrary gas composition is prohibitive if one relies on GCMC simulations alone, and it would be virtually impossible to rely on experimental data. To overcome this challenge, the Ideal Adsorbed Solution Theory (IAST) developed by Myers and Prausnitz[37] has become the most widely used tool. IAST uses pure component adsorption data to predict mixture behavior. The main equations of IAST are as follows, with all notation provided in Table 1.

$$P\Phi_i y_i = f_i^{\circ} x_i \tag{1}$$

$$\pi_i^{\circ}\left(f_i^{\circ}\right) = \frac{RT}{A}\int_{t=0}^{f_i^{\circ}} n_i^{\circ}(t)\,\mathrm{d}\ln t \tag{2}$$

$$\pi_i^{\circ}(f_i^{\circ}) = \pi_j^{\circ}(f_j^{\circ}) \tag{3}$$

$$\frac{1}{n_{\mathrm{a,u.c.}}} = \sum_i \frac{x_i}{n_i^{\circ}(f_i^{\circ})} \tag{4}$$

IAST assumes that the adsorbed phase can be treated as an ideal solution, *i.e.* adsorbed phase activity coefficients of unity, and uses the equality of fugacities in the two phases (eqn (1)) to relate the gas phase composition y_i and the adsorbed phase composition x_i. Equilibrium also requires that the spreading pressures of all species, as defined by eqn (2), are equal (eqn (3)). With eqn (4), one can also obtain the total amount of adsorbed gas molecules n_a. The Peng–Robinson equation of state is used to calculate the gas-phase fugacity coefficients Φ_i. For use in our model, we obtained analytical expressions of the adsorption isotherms of the pure components by fitting adsorption data to the classical Langmuir adsorption equation. For HKUST-1, the isotherms were obtained from adsorption measurements (see ESI†), and for all other MOFs the pure-component isotherms were obtained from GCMC simulations. The simulations were performed with the RASPA code.[38] MOF frameworks were treated as rigid and the gas molecules were allowed to be flexible. A united atom model was used for the alkanes, and universal force field (UFF)[39] and TraPPE force field[40] parameters were used for MOF atoms and alkane molecules, respectively. Further simulation details are provided in the ESI.† As an example, the simulated methane, ethane, and propane single-component adsorption isotherms in the MOF NU-125 are shown in Fig. 1. This MOF is an attractive structure for preliminary testing of our methods due to the excellent agreement between its simulated and measured methane adsorption isotherms, which is also shown in Fig. 1.[24]

IAST has been shown in the literature to work well for hydrocarbon adsorption in MOFs.[41,42] Some validation data for the application of IAST to adsorption of hexane isomer mixtures in zeolites and MOFs are included in the ESI.† Furthermore, as a

Table 1 Notation

Variables	Definitions
P	Total pressure
Φ_i	Fugacity coefficient of component i in the gas phase
y_i	Mole fraction of component i in the gas phase
f_i°	Equilibrium fugacity of pure i corresponding to spreading pressure
x_i	Mole fraction of component i in the adsorbed phase
π_i°	Spreading pressure of component i
R	Gas constant
T	Absolute temperature
A	Specific area of adsorbent
$n_i^{\circ}(f)$	Number of molecules of component i adsorbed per unit cell at fugacity f in pure component isotherm
$n_{\mathrm{a,u.c.}}$	Total number of molecules of all species per unit cell in the adsorbed phase
n_{a}	Total number of molecules in the adsorbed phase
n_g	Total number of molecules in the gas phase
n_i^{pre}	Number of molecules of component i in the tank left from the previous operating cycle
$\frac{n_i^{\mathrm{pipeline}}}{n_j^{\mathrm{pipeline}}}$	Ratio of number of molecules of component i over number of molecules of component j in the natural gas pipeline
M_i	Molecular weight of component i
m	Total mass of gas (including all components) inside the tank, including adsorbed and gas phases
t	Time
$\dot{m}$	Gravimetric fuel consumption rate

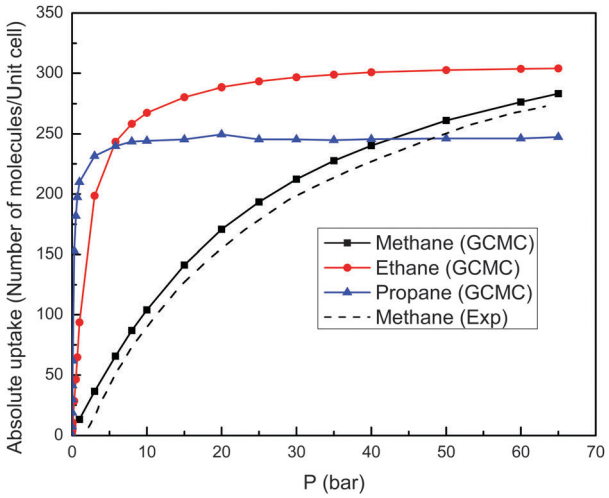

Fig. 1 Simulated methane, ethane, and propane single-component adsorption isotherms in NU-125 at 298 K. The experimental methane isotherm is also shown for comparison.[24]

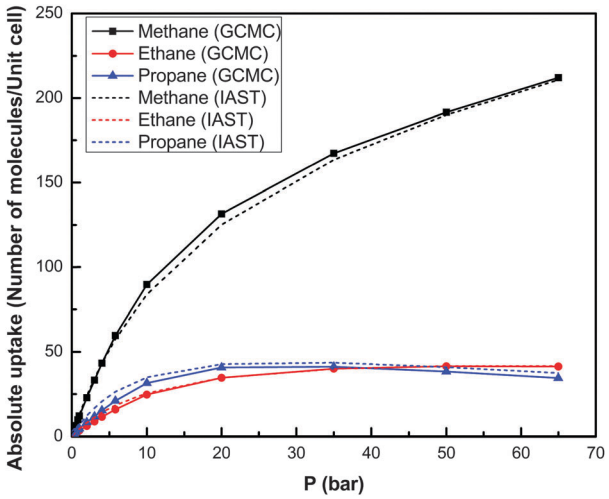

Fig. 2 Simulated methane, ethane and propane (mole fractions: 0.96, 0.033, 0.007) mixture isotherms (solid lines) and IAST predictions (dash lines) in NU-125 at 298 K.

test of IAST in our particular system, Fig. 2 shows that there is good agreement between isotherms obtained directly from GCMC mixture simulations and isotherms obtained by applying IAST on pure component simulated isotherms. The case illustrated in Fig. 2 corresponds to adsorption of a 96% methane, 3.3% ethane, and 0.7% propane mixture in the MOF NU-125.

ANG tank model

A typical ANG tank with adsorbent particles can be schematized as in Fig. 3. Due to packing inefficiencies, there is void space (white) between the adsorbent particles (green), in which the gas phase resides. In accordance with the parameters used by ARPA-E,[1] we assume a packing loss, *i.e.* packed bed porosity, of 25% due to unoccupied space in between MOF particles inside the ANG tank.

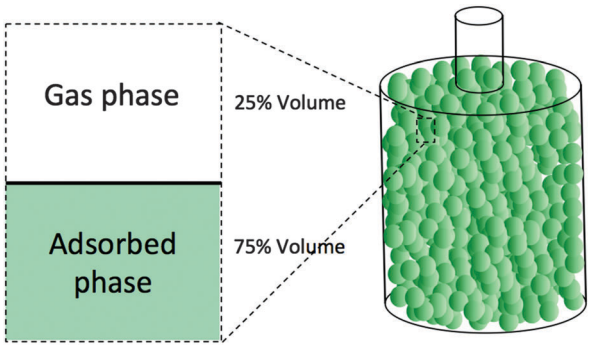

Fig. 3 The scheme of a simplified ANG vehicle tank.

For the tank model itself, we implement some simplifications: (i) we assume a slow filling process, which allows us to ignore heat effects and assume isothermal conditions within the ANG tank. One would expect this scenario to occur in home-filling stations. (ii) We neglect pressure and concentration gradients inside the tank. (iii) The gas phase and the adsorbed phase are assumed to reach equilibrium instantaneously during the adsorption or desorption process. This assumption is supported by molecular dynamics simulations that predict rapid diffusion of alkanes in some typical MOFs.[43] More detailed justification of the assumptions adopted in the model can be found in the ESI.†

An operating cycle of the tank consists of two processes, namely adsorption (filling) and desorption (delivering), which are governed by two different sets of mass conservation equations. During the adsorption process, the inlet flow from the natural gas pipeline can be assumed to have a constant molar composition (96% methane, 3.3% ethane, and 0.7% propane). As the adsorption progresses, the tank internal pressure increases, and the amount and composition of both gas and adsorbed phases inside the tank change simultaneously until the storage pressure (65 bar) is reached. Based on the mass conservation law, at any pressure, the system should follow the equation:

$$\frac{x_i n_a + y_i n_g - n_i^{pre}}{x_j n_a + y_j n_g - n_j^{pre}} = \frac{n_i^{pipeline}}{n_j^{pipeline}} \quad (5)$$

Once the pressure reaches 65 bar, we start the desorption process (delivering fuel to the engine) until the delivery pressure (5.8 bar) is reached. One can assume a constant mass flow rate during this process provides an approximately constant energy flow rate to the engine since the composition of the gas injected to the engine does not change dramatically, which ensures that the vehicle can perform similarly to a gasoline-powered car. Accordingly, the desorption process should follow:

$$\sum_i M_i (x_i n_a + y_i n_g) = m \quad (6)$$

$$\frac{dm}{dt} = \dot{m} \quad (7)$$

Other parameters used in the model are taken from the literature. We use a 152 L (40.15 gallon) ANG tank (data from a 3M commercial NG tank) and a fuel consumption rate equivalent to 0.0009 liter

of gasoline per s based on a 5 km driving test in an urban area at an average speed of 21.4 mph (including stops).[44] Based on the equations and methods described above, we developed a series of Matlab routines to solve the set of differential algebraic equations and calculate different properties of the ANG tank system at any instant during the operating cycles. The original code can be found in the ESI.†

Results and discussion

Model results for five promising MOFs based on pure methane storage

With the ANG tank model, we first tested the performance of five of the best MOFs for methane storage (based on their volumetric deliverable capacities for pure methane): HKUST-1, IRMOF-1, NU-111, NU-125 and NU-800. The goal was to determine if these materials can be expected to retain their promising performance in an ANG system with higher hydrocarbons in the natural gas. The properties of these five MOFs are listed in Table 2. From Table 2 it is apparent that GCMC simulations are rather inaccurate to describe the adsorption behavior of HKUST-1. Based on this observation, we opted to measure single-component methane, ethane, and propane isotherms in HKUST-1 and use these data as input for the ANG tank model subroutines for this material. More details about the experimental measurements on HKUST-1 are included in the ESI.†

The energy delivered to the engine per liter of tank can be calculated by adding the delivered amounts of methane, ethane, and propane multiplied by their respective heats of combustion. On the first adsorption/desorption cycle, the MOFs can in some cases deliver more energy than in the absence of higher alkanes due to the ethane and propane, which have higher heats of combustion than methane, being delivered to the engine (see Fig. S3, ESI†). However, upon additional cycles, the overall trend is that the higher alkanes start to accumulate in the MOF particles without being released to the engine. The accumulation of these species is apparent in Fig. 4, which shows how the overall (adsorbed plus gas phase) molar composition inside the ANG tank at the end of each desorption cycle changes when, for instance, NU-125 is used as the adsorbent material. Recall that the pipeline concentration used in these calculations is 96% methane, 3.3% ethane, and 0.7% propane. The observed behavior is representative of all MOFs investigated here and shows that the mole fractions of ethane and propane inside the tank increase until eventually they reach what we will refer to as a ''cyclic steady state''.

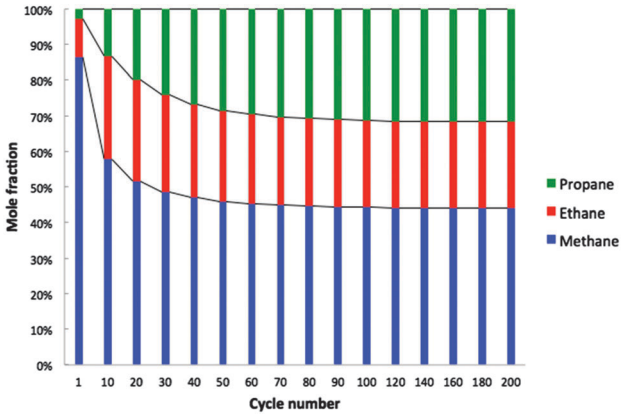

Fig. 4 Mole fractions of three components in the tank (gas phase plus adsorbed phase) at the end of each cycle (at 5.8 bar) in NU-125.

The expected decrease in energy delivered to the engine due to ethane and propane accumulation, which takes up pore space that can be no longer used to adsorb methane, is illustrated in Fig. 5. It shows the change in deliverable energy during the first 200 operating cycles of an ANG tank using NU-125 or HKUST-1 as adsorbent materials. Let us focus first on the NU-125 system. In the first cycle, this system initially delivers 5.96 MJ L^{-1} of tank, but this number decreases up to ~15% during subsequent cycles, finally delivering 5.08 MJ L^{-1} of tank during the cyclic steady state regime. This clearly shows that even the small amounts of higher hydrocarbons in commercial natural gas can have a significant impact on the performance of the system. Furthermore, this impact can vary for different materials. Notice in Fig. 5 that NU-125 and HKUST-1 initially deliver very similar amounts of energy per liter of tank, but the energy delivered to the engine decreases more sharply (up to ~32%) for the HKUST-1-based system, which only delivers 3.96 MJ L^{-1} of tank during the cyclic steady state regime. This result highlights the importance of evaluating adsorbent materials at realistic operating conditions.

Based on further analysis, we believe that the reason for the significant decrease in performance for the HKUST-1 system is the geometrical structure of the pores. The calculated pore size distribution of HKUST-1 (shown in Fig. S4, ESI†) shows three types of cavities, with the smallest one having a diameter of 5.5 Å. As we will further elaborate in the next section, the presence of

Table 2 BET surface areas, helium void fractions, pore volumes and the deliverable methane uptakes of the selected MOFs

MOFs	N_2 BET (m^2 g^{-1}) exp/calcd	Helium void fraction calcd	N_2 pore volume (cc/g) exp/calcd	Del. methane uptake[a] (cc/cc of adsorbent) exp/calcd	References for exp data
HKUST-1	1850/2064	0.76	0.78/0.78	184/158[b]	15
IRMOF-1	4140/3379	0.83	1.44/1.36	185/189[c]	10
NU-800	3149/3551	0.81	1.34/1.44	167/187[d]	25
NU-125	3120/3680	0.85	1.29/1.32	174/184[b]	15
NU-111	4930/4650	0.88	2.09/2.03	174/168[b]	15

[a] The deliverable methane uptake is between 65 bar and 5.8 bar at 298 K. [b] The calculated numbers are from the simulations carried out in this work using the simulation setting introduced in the ESI. [c] Calculated IRMOF-1 number is from ref. 29. [d] Calculated NU-800 number is from ref. 25.

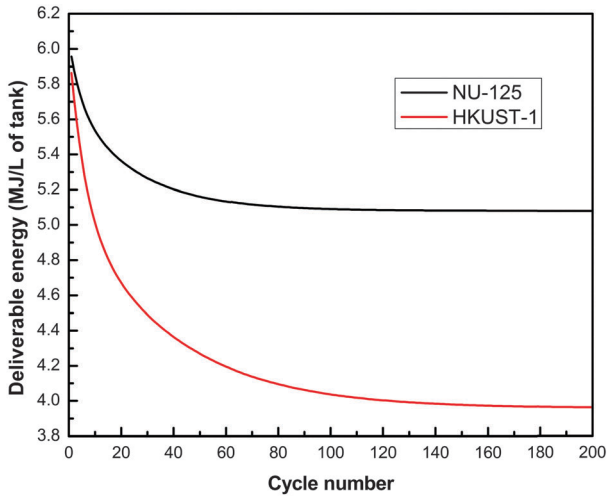

Fig. 5 Deliverable energy of each cycle in NU-125 and HKUST-1 (65–5.8 bar). For comparison, the deliverable energy of CNG (250–5.8 bar) is 9.0 MJ L^{-1} of tank.

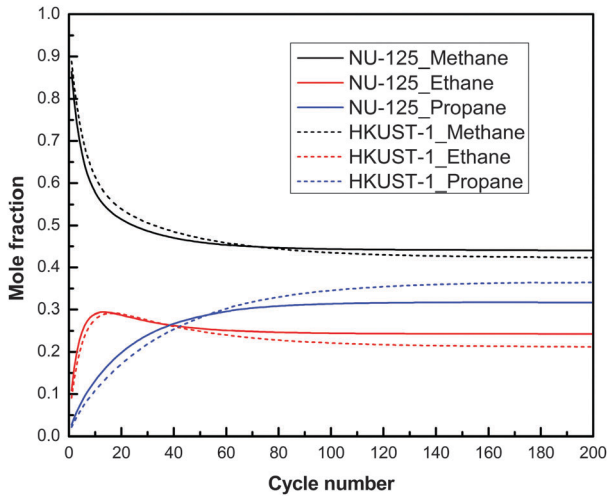

Fig. 6 Mole fractions of three components in the ANG tank (gas phase plus adsorbed phase) at the end of each cycle in NU-125 and HKUST-1.

such small cavities is detrimental to the performance of MOFs in general for natural gas storage. The smallest HKUST-1 cavities have particularly strong interactions with ethane and propane, because pore confinement effects are stronger than for methane. Indeed, by examining snapshots (see Fig. S5, ESI†) from the GCMC simulations of methane–ethane–propane mixture adsorption in HKUST-1 (using the same concentration as mentioned), we observe that at delivery pressure (5.8 bar) each small cavity already hosts one propane molecule, blocking adsorption of methane or ethane molecules. In this strong adsorption scenario, propane molecules cannot be driven out of the small cavities at the 5.8 bar delivery pressure. Fig. 6 compares the mole fractions of the three components in the tank at the end of each of 200 cycles between NU-125 and HKUST-1. The propane mole fraction is higher in HKUST-1 (~38%) than in NU-125 (~32%) during the steady state, which agrees with the sharper decrease in deliverable energy for HKUST-1.

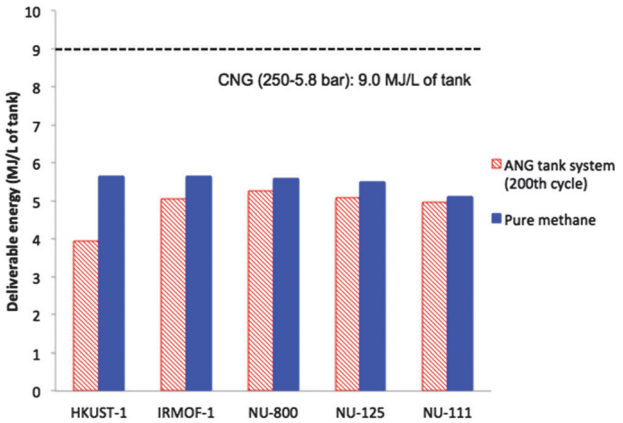

Fig. 7 Predicted deliverable energy between 65 bar and 5.8 bar for pure methane and natural gas mixtures in the five selected MOFs.

Fig. 7 shows the deliverable energy at the "cyclic steady state" for the five MOFs detailed in Table 2. While Fig. S3 (ESI†) shows that for the first cycle the deliverable energy can increase due to the presence of higher alkanes, after 200 cycles, there is always a negative impact on the deliverable energy compared to pure methane adsorption. Based on the calculations with our model, the MOF NU-800, among the materials in Table 2, is predicted to perform the best under realistic operating conditions in an ANG tank.

Computational screening of 120 synthesized MOFs

We also used the ANG tank model to conduct a computational screening of a population of 120 synthesized MOFs to (i) search for even better MOF candidates for use in ANG tanks working with realistic fuel compositions and (ii) get more insights and correlations between the MOF structures and their performance. This collection of structures consists of the five MOFs in Table 2 and an additional 115 synthesized MOFs extracted from the CoRE MOF database, which was generated by Chung *et al.* based on structures in the Cambridge Crystallographic Data Centre (CCDC) database.[29] The population of MOFs selected is dominated by materials with high predicted methane deliverable capacities, but also includes MOFs with lower methane deliverable capacities to help provide a broader view in terms of structure–property relationships. The most interesting relationships are plotted in Fig. 8 (the CCDC structure IDs of these 120 MOFs and their adsorption data, and all the other correlations can be found in the ESI†).

While our tank model allows us to calculate the deliverable energy of the ANG system at any instant, there are three values that are of special interest: (i) the deliverable energy of the first cycle, (ii) the cumulative deliverable energy, or the sum of the deliverable energy over all 200 cycles, and (iii) the deliverable energy at the steady state (at 200th cycle). The deliverable energy of the first cycle correlates linearly with the (pure) methane deliverable capacity (see Fig. S6, ESI†), indicating that the effect of impurities becomes more important only after a few operating cycles. To assess the performance of an adsorbent material in an ANG system one would like to know the total amount of energy

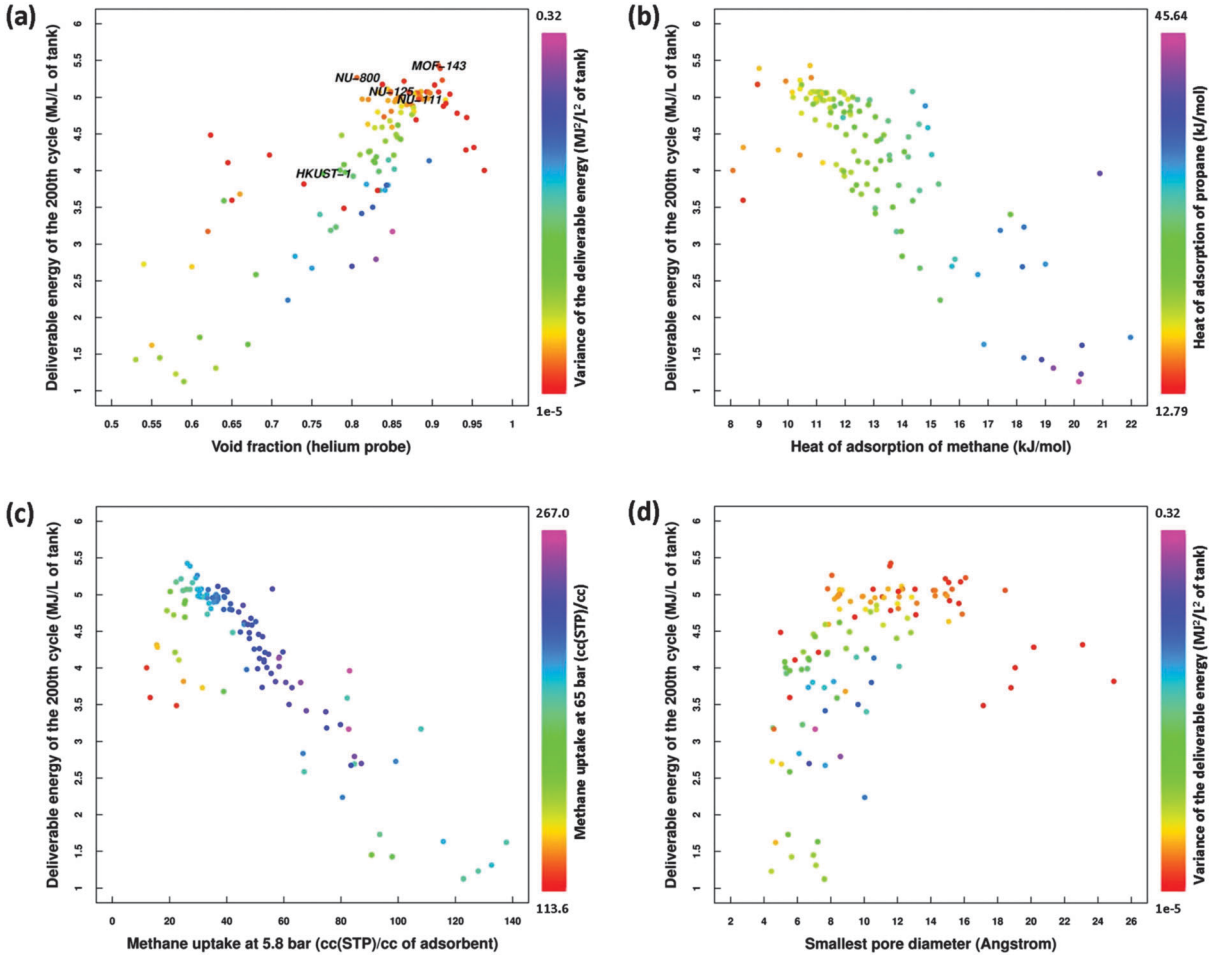

Fig. 8 Correlations between the deliverable energy at the 200th cycle and various MOF properties: (a) helium void fraction; (b) methane heat of adsorption; (c) volumetric methane uptake at 5.8 bar and 298 K; (d) smallest pore diameter of the MOF (based on the calculated pore size distribution). Each point in the plots corresponds to a MOF and is colored according to: (a) and (d) variance of the deliverable energy over the 200 cycles; (b) propane heat of adsorption; (c) volumetric methane uptake at 65 bar and 298 K.

delivered to the engine during a certain period of operation, *i.e.*, the cumulative deliverable energy. However, we found a linear correlation between the deliverable energy at the last (200th) cycle and the cumulative deliverable energy (see Fig. S7, ESI†) and will therefore focus on the former.

Fig. 8a shows the correlation between the deliverable energy at the last cycle and the calculated helium void fraction. Among the 120 tested MOF materials, the best candidate was found to be MOF-143, which was reported by Furukawa *et al.*[45] It should be kept in mind that this result is based on simulations using the perfect crystal structure. For MOF-143, to our knowledge, a viable method for removing solvent, while retaining the porosity promised by X-ray crystallography, has not yet been reported. NU-800, NU-125, and IRMOF-1 still perform relatively well and are ranked 2nd, 8th, and 14th, respectively, among the screened MOFs. In agreement with the discussion in the previous section, HKUST-1 is ranked 84th despite being one of the very best MOFs in terms of pure methane deliverable capacity. Table 3 summarizes important values and rankings for some notable MOFs. Interestingly, some members of the IRMOF family appear in the top five. Fig. 8a also shows that the best MOFs based on deliverable energy at the last cycle tend to have helium void fractions around 0.9, which is somewhat higher than for the best materials based on methane deliverable capacity[27–29] or methane adsorption at 35 bar.[20] This shift of the optimal void fraction toward higher values can be explained by the fact that structures with void fractions around 0.9 tend to have larger pores. This reduces confinement effects and effectively weakens the interaction between ethane and propane and the pore walls, *i.e.* the opposite of what happens for HKUST-1. The colors in Fig. 8a denote the variance of the deliverable energy, with higher values indicating higher decrease in performance with respect to the first cycle. A variance of zero indicates that the deliverable energy curve of the system (as those shown in Fig. 5 for NU-125 and HKUST-1) is completely flat. It is apparent, then, that the best MOFs in Fig. 8a have low variances, indicating they are less affected or poisoned by the presence of hydrocarbon impurities in the fuel mixture.

Ideally, one would like to optimize the methane heat of adsorption in a MOF material, while decreasing the ethane and

Table 3 Calculation results and rankings of some important MOFs from the 120 screened materials[a]

MOFs	Ranking NG[b]	Ranking methane[c]	Del. energy 200th cycle (MJ L^{-1} of tank)	Methane uptake 5.8 bar (cc/cc of adsorbent)[d]	Methane uptake 65 bar (cc/cc of adsorbent)[d]	Del. methane uptake 65–5.8 bar (cc/cc of adsorbent)[d]	Ref.[e]
MOF-143	1	39	5.43	26	208	182	45
NU-800	2	12	5.26	30	217	187	25
IRMOF-14	3	49	5.23	29	210	181	7
IRMOF-20	4	67	5.22	24	199	175	46
MIL-100	5	76	5.17	22	191	169	47
NU-125	8	25	5.08	56	240	184	24
IRMOF-1	14	8	5.07	33	222	189	7
NU-111	32	77	4.97	32	200	168	23
JUC-101	74	1	4.13	58	258	200	48
HKUST-1	84	26	3.96	83	267	184	49

[a] All numbers reported in this table are calculation results except for the methane uptakes of HKUST-1. [b] Based on the deliverable energy of the 200th cycle in the 120 MOFs. [c] Based on the pure methane deliverable volumetric uptakes. [d] Most of the data are from ref. 29. NU-800 numbers are from ref. 25. HKUST-1 results are based on experimental data. NU-125 and NU-111 numbers are calculated in this work using the same simulation setting mentioned in the ESI. [e] The references in which the crystal structures used in this work were reported for these MOFs.

propane heats of adsorption. However, these quantities are strongly coupled. Fig. 8b shows the optimal methane heat of adsorption for operating in an ANG tank with impurity-containing fuels ($\sim$10 kJ mol^{-1}) is somewhat lower than the one observed for MOFs adsorbing pure methane.[14,15,27] This is because moderately reducing the methane heat of adsorption is accompanied by a reduction of the propane and ethane heats of adsorption, which reduces the poisoning effect (notice how the point colors indicating lower propane heats of adsorption are toward the left of the plot). However, if the methane heat of adsorption is too low, not enough methane is adsorbed and even without poisoning the performance of the MOF is poor. Fig. 8c illustrates this situation. The methane heat of adsorption correlates well with methane uptake at low pressure (not shown), and even with only 120 evaluated MOF structures, we can clearly see a sharp peak in the deliverable energy of the 200th cycle at a methane uptake of $\sim$30 cc(STP) per cc of adsorbent at 5.8 bar. At the right of 30 cc(STP) per cc of adsorbent, we have MOFs that have high pure methane uptake at 65 bar (see color scale in Fig. 8c), which indicates a high affinity for methane, but susceptibility to poisoning. At the left of 30 cc(STP) per cc of adsorbent, we have MOFs that have low pure methane uptake at 65 bar, which indicates low susceptibility to poisoning, but low affinity for methane. In summary, between two MOFs with similar pure methane deliverable capacities, the one with the shallower methane isotherm is expected to perform better in conditions where there are higher alkanes in the gas.

In analysing Fig. 8d, it is appropriate to revisit the discussion about HKUST-1 in the previous section. We noted that the susceptibility of HKUST-1 to poisoning was due to the small $\sim$5.5 Å cavities. Indeed, Fig. 8d shows that almost all the poor-performing structures (including HKUST-1) have their smallest cavities in the 4–10 Å range. This agrees with our hypothesis that these small cavities can trap the higher alkane molecules leading to their accumulation after several operating cycles. It is thus crucial to avoid designing MOF materials with such small cavities, even if they also have larger cavities as occurs for MOFs with multimodal pore distributions. The colors in Fig. 8d, which as in Fig. 8a indicate the variance of the deliverable energy, show that most of the materials with low susceptibility to poisoning (red points) are located in the region corresponding to MOFs whose smallest cavities are larger than 10 Å. Other plots included in the ESI† show additional correlations and optimal intervals. For instance, the optimal values of volumetric and gravimetric surface area are 1850 m^2 cm^{-3} and 5500 m^2 g^{-1}, respectively.

The sensitivity of the system with respect to the packing loss

As noted in the modeling section, we applied a packing loss of 25% of the total volume of the tank in the model. However, one can vary this number by using different synthesis techniques or particle filling methods. Is the ANG system sensitive to this variable and how much can we enhance the performance of MOFs by improving the packing efficiency? Fig. 9 shows the results based on two typical structures, NU-125 and the best candidate from the more extensive screening, MOF-143. Interestingly, it is observed that as the packing loss is decreased from 50% to 0%, the deliverable energy of the 200th cycle of both MOFs

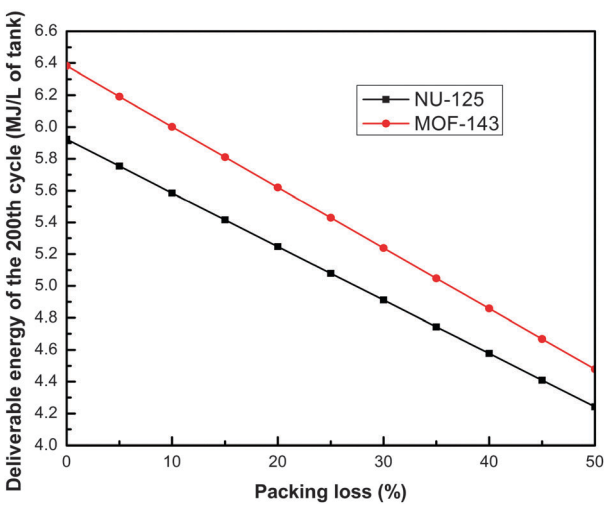

Fig. 9 The deliverable energy of the 200th cycle with different packing loss values.

increases linearly. It should be noticed that, with a packing loss of 0%, indicating that we have a crystal monolith inside the tank, MOF-143 can deliver 6.4 MJ L^{-1} of tank to the engine.

Conclusions

In this work, we combined molecular simulations and macroscopic thermodynamics to develop a theoretical model for an ANG tank to study the effect of the higher hydrocarbons, especially ethane and propane, on the performance of an ANG system. We used this model to test a series of promising MOF materials for natural gas storage and observed the accumulation of the higher alkanes in the MOF adsorbents over many cycles and the formation of a "cyclic steady state". The results show that some materials that are excellent for storage of pure methane, such as HKUST-1, are not suitable for real natural gas storage due to the poisoning effect of the higher alkanes. Furthermore, we conducted a computational screening of 120 existing MOFs and were able to identify some top MOF materials for natural gas storage including NU-series MOFs (NU-800 > NU-125 > NU-111) and some IRMOFs (IRMOF-14 > IRMOF-20 > IRMOF-1). The best MOF candidate identified is MOF-143, with a deliverable energy of 5.43 MJ L^{-1} of tank during the steady state, which unfortunately is still considerably below the storage target of 9.0 MJ L^{-1} of tank. With MOF-143 filled in the vehicle tank, one could drive about 160 miles with one tank of adsorbed natural gas at an average speed of 21.4 mph. A sensitivity analysis of the ANG system with respective to the packing loss was carried out and the deliverable energy decreases linearly with the packing loss values. If the tank could be filled with a monolith of the best MOF candidate, MOF-143, which would correspond to a packing loss of zero, one could enhance the deliverable energy of the 200th cycle to 6.4 MJ L^{-1} of tank, which would allow one to drive about 187 miles with one tank of ANG.

Additionally certain correlations between the deliverable energy and MOF properties were discovered. The optimal MOF candidate for natural gas storage should have a helium void fraction of 0.9, a volumetric surface area of 1850 m^2 cm^{-3}, a gravimetric surface area of 5500 m^2 g^{-1} and a heat of adsorption of methane at low loading of 10 kJ mol^{-1}. MOFs containing small cavities with diameters of 4 to 10 Å should be avoided due to their strong interactions with ethane and propane molecules. For high-throughput screening, one would like to avoid the lengthy calculations presented here, and our results suggest that if only pure methane adsorption information is available, a straightforward way to find good candidates, which will perform well with real natural gas, is to search for MOFs having linear methane isotherms with relatively large slopes. Candidates identified in this way can then be evaluated with our model or tested in cyclic adsorption studies with real natural gas.

Acknowledgements

We acknowledge that the work presented herein was funded by the Advanced Research Projects Agency-Energy (ARPA-E), U.S. Department of Energy, under Award Number DE-AR0000248. Thanks also go to Dr Yongchul G. Chung for his assistance with the CoRE MOF database.

Notes and references

1 ARPA-E Methane Opportunities for Vehicular Energy (MOVE), 2012.
2 D. Lozano-Castelló, J. Alcañiz-Monge, M. A. d. l. Casa-Lillo, D. Cazorla-Amorós and A. Linares-Solano, *Fuel*, 2002, **81**, 1777–1803.
3 V. C. Menon and S. Komarneni, *J. Porous Mater.*, 1998, **5**, 43–58.
4 M. O'Keeffe and O. M. Yaghi, *Chem. Rev.*, 2012, **112**, 675–702.
5 R. L. Martin, L. C. Lin, K. Jariwala, B. Smit and M. Haranczyk, *J. Phys. Chem. C*, 2013, **117**, 12159–12167.
6 M. Kondo, T. Yoshitomi, K. Seki, H. Matsuzaka and S. Kitagawa, *Angew. Chem., Int. Ed.*, 1997, **36**, 1725–1727.
7 M. Eddaoudi, J. Kim, N. Rosi, D. Vodak, J. Wachter, M. O'Keeffe and O. M. Yaghi, *Science*, 2002, **295**, 469–472.
8 T. Düren, L. Sarkisov, O. M. Yaghi and R. Q. Snurr, *Langmuir*, 2004, **20**, 2683–2689.
9 U. Stoeck, S. Krause, V. Bon, I. Senkovska and S. Kaskel, *Chem. Commun.*, 2012, **48**, 10841–10843.
10 J. A. Mason, M. Veenstra and J. R. Long, *Chem. Sci.*, 2014, **5**, 32–51.
11 S. Ma and H. Zhou, *Chem. Commun.*, 2010, **46**, 44–53.
12 Y. He, W. Zhou, T. Yildirim and B. Chen, *Energy Environ. Sci.*, 2013, **6**, 2735–2744.
13 H. Wu, J. M. Simmons, Y. Liu, C. M. Brown, X. Wang, S. Ma, V. K. Peterson, P. D. Southon, C. J. Kepert, H. Zhou, T. Yildirim and W. Zhou, *Chem. – Eur. J.*, 2010, **16**, 5205–5214.
14 T. A. Makal, J. Li, W. Lu and H. Zhou, *Chem. Soc. Rev.*, 2012, **41**, 7761–7779.
15 Y. Peng, V. Krungleviciute, I. Eryazici, J. T. Hupp, O. K. Farha and T. Yildirim, *J. Am. Chem. Soc.*, 2013, **135**, 11887–11894.
16 O. O. Adisa, B. J. Cox and J. M. Hill, *Nanoscale*, 2012, **4**, 3295–3307.
17 W. Zhou, *Chem. Rec.*, 2010, **10**, 200–204.
18 L. Zhou, J. Liu, W. Su, Y. Sun and Y. Zhou, *Energy Fuels*, 2010, **24**, 3789–3795.
19 H. Furukawa and O. M. Yaghi, *J. Am. Chem. Soc.*, 2009, **131**, 8875–8883.
20 C. E. Wilmer, M. Leaf, C. Y. Lee, O. K. Farha, B. G. Hauser, J. T. Hupp and R. Q. Snurr, *Nat. Chem.*, 2012, **4**, 83–89.
21 X. Duan, J. Yu, J. Cai, Y. He, C. Wu, W. Zhou, T. Yildirim, Z. Zhang, S. Xiang, M. O'Keeffe, B. Chen and G. Qian, *Chem. Commun.*, 2013, **49**, 2043–2045.
22 B. Li, H. Wen, H. Wang, H. Wu, M. Tyagi, T. Yildirim, W. Zhou and B. Chen, *J. Am. Chem. Soc.*, 2014, **136**, 6207–6210.
23 Y. Peng, G. Srinivas, C. E. Wilmer, I. Eryazici, R. Q. Snurr, J. T. Hupp, T. Yildirim and O. K. Farha, *Chem. Commun.*, 2013, **49**, 2992–2994.

24 C. E. Wilmer, O. K. Farha, T. Yildirim, I. Eryazici, V. Krungleviciute, A. A. Sarjeant, R. Q. Snurr and J. T. Hupp, *Energy Environ. Sci.*, 2013, **6**, 1158–1163.
25 D. A. Gomez-Gualdron, O. V. Gutov, V. Krungleviciute, B. Borah, J. E. Mondloch, J. T. Hupp, T. Yildirim, O. K. Farha and R. Q. Snurr, *Chem. Mater.*, 2014, **26**, 5632–5639.
26 F. Gándara, H. Furukawa, S. Lee and O. M. Yaghi, *J. Am. Chem. Soc.*, 2014, **136**, 5271–5274.
27 D. A. Gomez-Gualdron, C. E. Wilmer, O. K. Farha, J. T. Hupp and R. Q. Snurr, *J. Phys. Chem. C*, 2014, **118**, 6941–6951.
28 R. L. Martin, C. M. Simon, B. Smit and M. Haranczyk, *J. Am. Chem. Soc.*, 2014, **136**, 5006–5022.
29 Y. G. Chung, J. Camp, M. Haranczyk, B. J. Sikora, W. Bury, V. Krungleviciute, T. Yildirim, O. K. Farha, D. S. Sholl and R. Q. Snurr, *Chem. Mater.*, 2014, **26**, 6185–6192.
30 W. E. Liss, W. H. Thrasher, G. F. Steinmetz, P. Chowdiah and A. Attari, Variability of Natural Gas Composition in Select Major Metropolitan Areas of the United States, PB92-224617, GRI, 1992.
31 S. M. P. Lucena, V. A. Gomes, D. V. Gonalves, P. G. M. Mileo and P. F. G. Silvino, *Carbon*, 2013, **61**, 624–632.
32 R. B. Rios, M. Bastos-Neto, M. R. Amora Jr., A. E. B. Torres, D. C. S. Azevedo and C. L. Cavalcante Jr., *Fuel*, 2011, **90**, 113–119.
33 E. J. Prosen and F. D. Rossini, *J. Res. Natl. Bur. Stand.*, 1945, **34**, 263–268.
34 B. Hardy, C. Corgnale, R. Chahine, M. Richard, S. Garrison, D. Tamburello, D. Cossement and D. Anton, *Int. J. Hydrogen Energy*, 2012, **37**, 5691–5705.
35 M. Farzaneh-Gord, S. Hashemi and A. Farzaneh-Kord, *World Appl. Sci. J.*, 2008, **5**, 143–149.
36 M. Farzaneh-Gord, *J. Theor. Appl. Mech.*, 2011, **41**, 21–36.
37 A. L. Myers and J. M. Prausnitz, *AIChE J.*, 1965, **11**, 121–127.
38 D. Dubbeldam, S. Calero, D. E. Ellis and R. Q. Snurr, *Mol. Simul.*, 2015, DOI: 10.1080/08927022.2015.1010082.
39 A. K. Rappe, C. J. Casewit, K. S. Colwell, W. A. Goddard III and W. M. Skiff, *J. Am. Chem. Soc.*, 1992, **114**, 10024–10035.
40 M. G. Martin and J. I. Siepmann, *J. Phys. Chem. B*, 1998, **102**, 2569–2577.
41 D. Dubbeldam, R. Krishna, S. Calero and A. O. Yazaydin, *Angew. Chem., Int. Ed.*, 2012, **51**, 11867–11871.
42 Z. R. Herm, B. M. Wiers, J. A. Mason, J. M. van Baten, M. R. Hudson, P. Zajdel, C. M. Brown, N. Masciocchi, R. Krishna and J. R. Long, *Science*, 2013, **340**, 960–964.
43 B. Borah, H. Zhang and R. Q. Snurr, *Chem. Eng. Sci.*, 2015, **124**, 135–143.
44 M. G. Lee, Y. K. Park, K. K. Jung and J. J. Yoo, *International Journal of u- and e-Service, Science and Technology*, 2011, **4**, 37–46.
45 H. Furukawa, Y. B. Go, N. Ko, Y. K. Park, F. J. Uribe-Romo, J. Kim, M. O'Keeffe and O. M. Yaghi, *Inorg. Chem.*, 2011, **50**, 9147–9152.
46 J. L. C. Rowsell and O. M. Yaghi, *J. Am. Chem. Soc.*, 2006, **128**, 1304–1315.
47 Q. Fang, G. Zhu, M. Xue, J. Sun, Y. Wei, S. Qiu and R. Xu, *Angew. Chem., Int. Ed.*, 2005, **44**, 3845–3848.
48 J. Jia, F. Sun, T. Borjigin, H. Ren, T. Zhang, Z. Bian, L. Gao and G. Zhu, *Chem. Commun.*, 2012, **48**, 6010–6012.
49 S. S. Y. Chui, S. M. F. Lo, J. P. H. Charmant, A. G. Orpen and I. D. Williams, *Science*, 1999, **283**, 1148–1150.

